THE JOURNAL OF PHYSICAL CHEMISTRY LETTERS
A JOURNAL OF THE AMERICAN CHEMICAL SOCIETY

pubs.acs.org/JPCL
Perspective

The Critical Role of nπ* States in the Photophysics and Thermally Activated Delayed Fluorescence of Spiro Acridine-Anthracenone

Larissa Gomes Franca, Yun Long, Chunyong Li, Andrew Danos, and Andrew Monkman*

Cite This: J. Phys. Chem. Lett. 2021, 12, 1490−1500
Read Online

ABSTRACT: The molecular photophysics and thermally activated delayed fluorescence (TADF) in spiro compounds are distinct because of the rigid orthogonal C−C bridging bond between donor and acceptor. The photophysics is found to be highly complex, with unprecedented multiple anti-Kasha emissions from three different singlet states, two of which are one-photon forbidden. The TADF mechanism is critically controlled by local acceptor nπ* states; the singlet nπ* state undergoes rapid intersystem crossing populating an energetically close acceptor ππ* triplet state. The acceptor triplet nπ* state couples nonadiabatically to a CT triplet state mediating reverse intersystem crossing. When the nπ* and CT states are energetically close, TADF is greatly enhanced with rISC rate reaching 10^7 s^{-1}. We observe neither DF from the singlet nπ* state nor electron transfer (ET) to form the ^{1}CT because there is no ET driving force; however, ET from the higher-energy donor singlet ππ* state readily occurs along with donor emission.

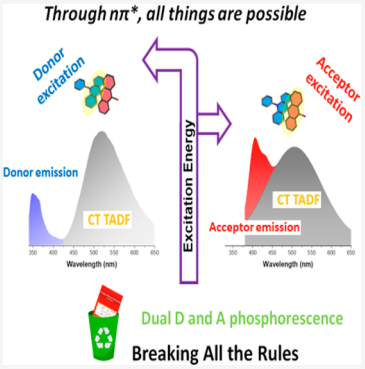

Organic light-emitting diodes (OLEDs) now underpin a large section of the display market because of their many appealing characteristics, including being high efficiency, flexible, and solution processable, and their ability to be fabricated on low-cost substrates.[1−4] Development of suitable emitters for OLEDs is fundamental in increasing their output efficiency and optimizing device performance. One of the key requirements is an emitter that utilizes triplet excited states to maximize the achievable internal quantum efficiency close to 100%. Phosphorescent materials currently used in OLED displays have provided one route, using heavy-metal-containing organic complexes to facilitate spin−orbit coupling and efficient spin-mixing to give efficient phosphorescence.[5,6] In addition, nonradiative decay of triplet excitons formed in the emission layer host material can be suppressed by ensuring that the triplet energy of the host is higher than that of the phosphorescent emitter.[7]

An alternative method for harvesting triplet states, thermally activated delayed fluorescence (TADF), has attracted tremendous interest for OLED applications by providing a means of harvesting triplet excitons without the need for rare and expensive heavy metals.[8,9] Thermal activation of triplet excitons causes them to undergo reverse intersystem crossing (rISC) back to the singlet manifold, producing delayed fluorescence. To achieve efficient rISC, TADF molecules must meet several key criteria, starting with a small S_1-T_1 energy gap, ΔE_{ST}. One way to achieve this is through a lowest-energy excited state of charge-transfer (CT) character. Charge-transfer states achieve effective separation of electron and hole wave functions and small associated ΔE_{ST} values, either by possessing structurally orthogonal D and A moieties (decoupling their individual electronic systems) or through a large spatial separation of D and A fragments (*e.g.*, in exciplexes[10]). Either approach results in minimal electron exchange interaction energy and a very small ΔE_{ST}, frequently <50 meV.[11−13] However, when the electron exchange energy is so small, the singlet (^{1}CT) and triplet (^{3}CT) orbitals become degenerate and transition between the two is spin-forbidden as no change in orbital angular momentum can occur.[14] To facilitate TADF a third triplet excited state, very close in energy to the ^{3}CT state but having different orbital character, is required to mix (nonadiabatically) with ^{3}CT to mediate a spin flip and couple the triplet back to the singlet manifold. This can be either a local triplet state (^{3}LE) or a higher-lying triplet CT state.[15]

An orthogonal N−C donor−acceptor bridge is typically used in TADF materials to give the appropriate energy level ordering, but such bonding is not a prerequisite for TADF.[8,9,16−18] While only a few examples have been reported, in spiro-linked D−A molecules the rigid and orthogonal donor−acceptor C−C bridge can yield efficient rISC.[19−21] This is very important as a bridging C−N bond between D and A in a typical D−A TADF material is considered to be a very weak bond, prone to degradation. This is one of the suspected main causes of the short lifetimes achievable by TADF emitters

Received: November 5, 2020
Accepted: January 28, 2021
Published: February 3, 2021

https://dx.doi.org/10.1021/acs.jpclett.0c03314
J. Phys. Chem. Lett. 2021, 12, 1490−1500

in devices. Moving away from this architecture, to a spiro system for example, could greatly enhance emitter lifetime, and this provides a very compelling motivation for these studies to provide a better understanding of spiro TADF emitters.

The spiro-linked acridine anthracenone derivative 10-phenyl-10*H*,10′*H*-spiro[acridine-9,9′-anthracen]-10′-one (ACRSA, Scheme 1) was one of the first reported spiro-linked

Scheme 1. Chemical Structure of ACRSA

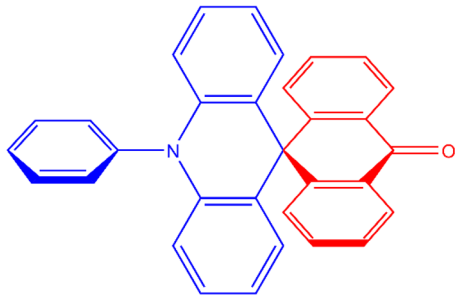

TADF materials. It showed efficient solution-state photoluminescence (PL efficiency of 81%), with similar performance (~75%) doped in the OLED host bis[2-(diphenylphosphino)-phenyl] ether oxide (DPEPO) leading to moderately high device EQE of 16.5% in the same host.[22,23] The generally moderate (but never outstanding) device performances reported for spiro-linked TADF materials (compared with up to 25% EQE in C−N linked D−A molecules) suggest a different photophysics and/or rISC mechanism may be active in the presence of the C−C spiro-bridge, warranting further investigation.

Lyskov and Marian have recently presented a very detailed quantum chemistry analysis of the ACRSA molecule. They highlight the complex interactions between charge transfer and local states, the role of state mixing (with high-lying excitonic transitions) that overcomes the forbidden nature of radiative decay from these states, and the potential for rapid nanosecond rISC mediated by n−π^* to π−π^* ISC transitions.[24] The excited states (calculated in a toluene environment) and a composite energy state diagram from their data, using their state nomenclature, are given in Supporting Scheme 1.

Applying a range of spectroscopic measurements to ACRSA, we uncover highly complex photophysics, in which several general principles of molecular spectroscopy are contravened. From such a "simple" molecule, the complexity of its multiple decay channels reflects the critical roles that nonadiabatic vibronic coupling and the nπ^* state of the acceptor have on molecular photophysics and also demonstrates the strongly decoupled nature of D and A units.

Applying a range of spectroscopic measurements to ACRSA, we uncover highly complex photophysics, in which several general principles of molecular spectroscopy are contravened.

Because of its CT excited states, the photophysics of ACRSA is highly dependent on the solvent environment. Starting with the absorption spectrum of ACRSA in toluene (Supporting Figure S1), two strongly allowed transitions are observed to have onset at 3.64 and 3.83 eV, ascribed as ground state $1^1A_1 \rightarrow 1^1B_2$ and $1^1A_1 \rightarrow 1^1B_1$, respectively, allowed π−π^* exciton transitions (Supporting Scheme 1).[24]

Following excitation at 330 nm (3.76 eV) into the 1^1B_1 state, the resulting emission of both aerated and degassed toluene solutions (Figure 1a,d) shows a very large Stokes shift with emission onset at 2.7 eV and a structureless Gaussian line shape, implying pure CT character. This corresponds to the $1^1A_2 \rightarrow 1^1A_1$ transition (Supporting Scheme 1), experimentally confirming that the 1^1A_2 is the lowest-energy singlet ^{1}CT state. Addition of oxygen results in a large reduction in the emission intensity, consistent with an oxygen-quenched delayed fluorescence (DF) component that otherwise dominates the total emission. The reduced ^{1}CT emission in aerated solution allows us to additionally detect the presence of a further high-energy emission band (onset, 3.7 eV). Upon comparing this emission to that previously observed in acridine[25] it is clear that this emission emanates from the acridine ^1LE_D $\pi\pi^*$ state (1^1B_1 in Supporting Scheme 1 and Figure S2). The fast radiative decay of this ^1LE_D excitonic state competes effectively with internal conversion (IC), electron transfer, and intersystem crossing (ISC) nonradiative decay channels. The $\pi\pi^*$ character is confirmed by the positive solvatochromic shift observed in this absorption band (Supporting Figure S3).

As both the emission of the ^1LE_D $\pi\pi^*$ state and a portion of the ^{1}CT emission are not fully quenched by oxygen, this indicates that the exciton can undergo electron transfer yielding the ^{1}CT state directly. High-energy triplet states formed by electron transfer and additionally by ISC from the ^1LE_D $\pi\pi^*$ state will cascade down to the lowest-energy triplet state—which can be harvested to give oxygen-sensitive TADF emission.

The relative yields of each emissive state for different excitation wavelengths are shown in Figure 2. Excitation of the solution below the onset of the ^1LE_D transition (>350 nm, 3.54 eV, Figure 1b,c) reveals emission from another new structured band (onset at 3.1 eV as well as weak ^{1}CT emission). As the ^1LE_D transition has already been identified, we propose that this new localized emission arises from the symmetry-forbidden ^1LE_A nπ^* state of the anthracenone acceptor unit, *i.e.*, from the $2^1A_2 \rightarrow 1^1A_1$ transition. Transitions between states of A_1 to A_2 symmetry are one-photon, dipole-forbidden; however, coupling with the high-energy $\pi\pi^*$ excitonic state can lend oscillator strength to these transitions.[24] On degassing the solution we again observe a large increase in the intensity of the ^{1}CT emission because of a DF contribution, such that the unaffected ^1LE_A nπ^* emission becomes barely visible by comparison (Figure 1e,f). Dual emission through different channels at both high (330 nm) and low (350 nm) excitation energies establishes ACRSA as a doubly anti-Kasha emitter.

As we observe emission from both ^1LE_A and ^{1}CT in aerated solution (380 nm excitation, well below the absorption tail of the ^1LE_D excitonic state), we must conclude that both states are directly populated, yielding prompt emission. Calculation of oxygen-quenched delayed CT emission contribution (Supporting Figure S4) shows that direct ^{1}CT absorption is more efficient at populating the ^{1}CT state than ET from the ^1LE_D exciton; 330 nm gives a PF/DF ratio of 6.8%, while at 380 nm PF/DF increases to 11.1% (lower triplet yield so lower DF). From the strong DF component we infer that the ^{1}CT−^{3}CT energy gap (1^1A_2−1^3A_2 gap, Supporting Scheme 1)

https://dx.doi.org/10.1021/acs.jpclett.0c03314
J. Phys. Chem. Lett. 2021, 12, 1490−1500

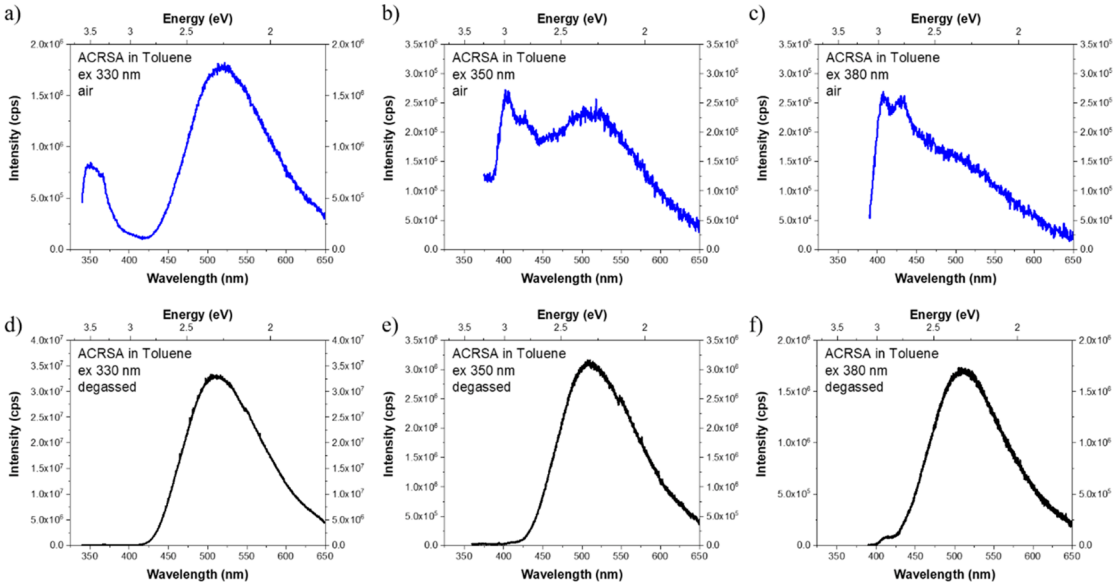

Figure 1. Steady-state emission from toluene solutions (50 μM) measured at three different excitation wavelengths: 330, 350, and 380 nm (non-normalized data). Top row spectra (a–c) are measured in aerated solution; bottom row (d–f) are measured in degassed solution showing the very strong delayed fluorescence contribution to emission, irrespective of excitation wavelength.

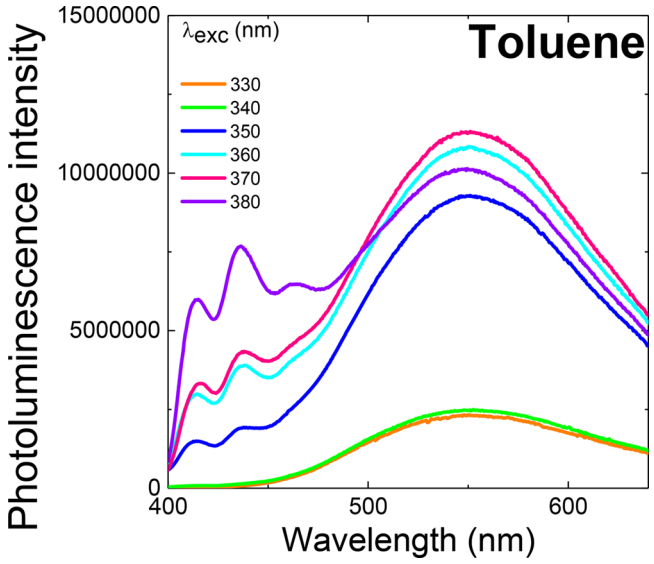

Figure 2. Relative PL emission yields from aerated ACRSA toluene solution (1 mg/mL) normalized by the absorbance at each excitation wavelength, showing low quantum yield from excitation *via* the acridine excitonic state (330 nm excitation) compared to excitation into the direct low-energy ^{1}CT and ^{1}LE$_A$ transitions (370 nm excitation).

must be small, indicating very low electron exchange energy from near degenerate orbitals. Consequently, ISC between ^{1}CT and ^{3}CT will be forbidden,[14,26] and the strong DF CT emission observed when exciting at ≥350 nm can arise only through the photoexcited ^{1}LE$_A$ state forming a large triplet population by ISC. Such efficient quenching by ISC—resulting in a large ^{3}CT population and strong DF—fully supports the proposal made by Lyskov and Marian[24] that the ^{1}LE$_A$ nπ* state couples strongly to a ^{3}LE$_A$ $\pi\pi$* triplet state (1^3A_1, Supporting Scheme 1) in competition with radiative decay.

These interpretations are further supported by excitation profiles measured at different emission collection wavelengths (Figure 3 and Supporting Figure S5). Monitoring emission from the ^{1}CT state (at 515 and 600 nm), we observe emission arising from excitation of both the ^{1}LE$_D$ excitonic state (at <350 nm) as well as direct excitation of the ^{1}CT (at ∼400 nm). Again, the CT emission is dominated by DF (degassed conditions), which is thoroughly quenched in aerated measurements. Monitoring at 412 nm (the peak of the ^{1}LE$_A$ nπ* emission), excitation into the ^{1}LE$_D$ excitonic state gives weak emission, which indicates active IC from ^{1}LE$_D$ $\pi\pi$* to ^{1}LE$_A$ nπ*. Much stronger ^{1}LE$_A$ nπ* emission is observed with excitation in the 350–400 nm range, resulting from direct ^{1}LE$_A$ nπ* excitation. The ^{1}LE$_A$ nπ* emission increases slightly on degassing, probably from enhancement of underlying delayed CT emission (with direct absorption from 350 to 415 nm). Excitation at wavelengths >425 nm yields no ^{1}LE$_A$ nπ* emission, although we do observe weak ^{1}CT emission (Supporting Figure S6), indicating that the onset of direct ^{1}CT absorption is at lower energy than the ^{1}LE$_A$ nπ* state. These excitation measurements demonstrate that excitation of the high-energy ^{1}LE$_D$ excitonic state gives rise to emission from three different singlet states simultaneously: ^{1}LE$_D$ exciton, ^{1}LE$_A$ nπ*, and ^{1}CT. While dual-emission TADF and room-temperature phosphorescent (RTP) materials are now frequently reported,[27−30] extreme anti-Kasha behavior such that a molecule is capable of emitting from three singlet excited states (^{1}LE$_D$ exciton, ^{1}LE$_A$, and ^{1}CT) simultaneously is exceedingly rare. We believe this is the first report of concurrent triple-pathway singlet emission from a single molecule.

Extending to solvents of different polarity, Figure 4 shows the emission spectra of ACRSA in MCH, toluene, and DCM (aerated and degassed) at different excitation wavelengths. Supporting Figure S7 directly compares emission between excitation at 330 and 380 nm in each solvent for additional clarity. In MCH and DCM, the same general trends are observed as in toluene. However, the structured emission from the local ^{1}LE$_A$ nπ* state is clearly not affected by polarity (Supporting Figure S8). In MCH the ^{1}CT emission is only

https://dx.doi.org/10.1021/acs.jpclett.0c03314
J. Phys. Chem. Lett. 2021, 12, 1490−1500

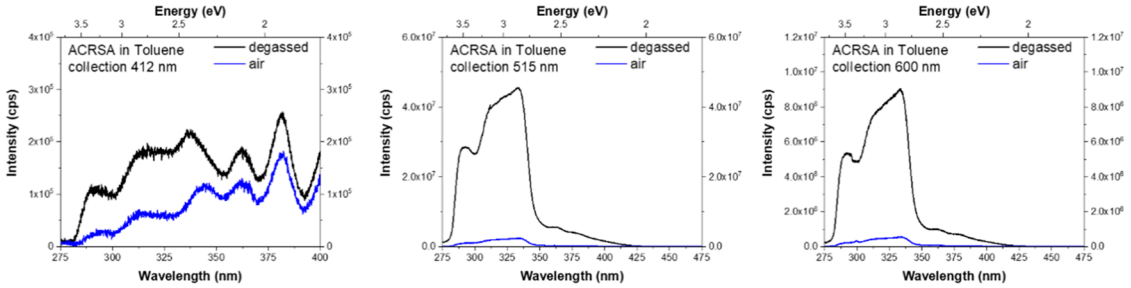

Figure 3. Excitation spectra from aerated and degassed ACRSA toluene solution (50 μM) showing the direct (≥350 nm excitation) and indirect population (from ^1LE_D, <350 nm excitation) of the ^1LE_A nπ^* and ^1CT states.

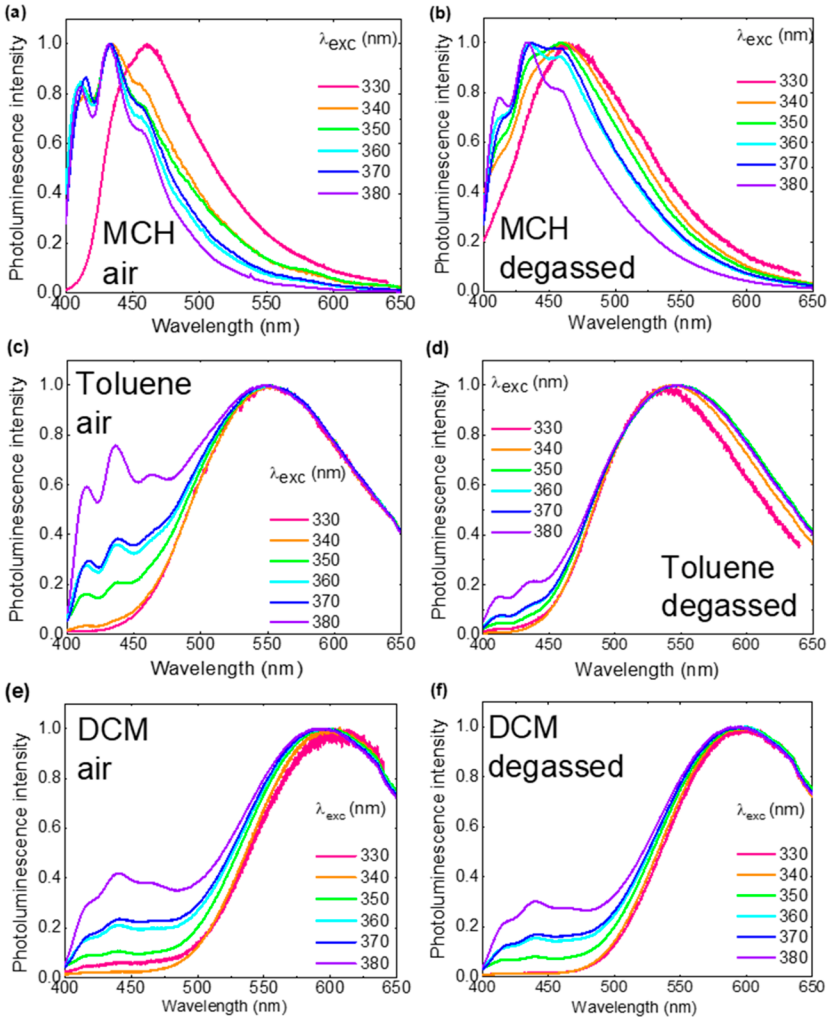

Figure 4. Emission spectra of ACRSA (1 mg/mL) in aerated and degassed solvents (a and b) MCH (ε = 2.02), (c and d) toluene (ε = 2.38), and (e and f) DCM (ε = 8.93) at different excitation wavelengths.

very weakly stabilized, lies underneath the local ^1LE_A nπ^* emission, but is readily distinguished by the strong CT emission observed with 330 nm excitation (into the ^1LE_D state). The appearance of the structured local emission increasing on removal of oxygen is in fact due to this underlying CT emission increasing (Supporting Figure S9). This is confirmed by the apparent relative decrease in local emission on degassing in DCM, where the CT band is red-shifted out from underneath the local emission band (but still partially overlapping) such that the true behavior of the local transition can been seen clearly.

It is interesting to compare this general emission behavior of ACRSA to its separate acridine donor and anthracenone acceptor units. Acridine emits at 337 nm (Supporting Figure S2), whereas anthracenone (or anthrone) is reported as nonemissive.[31] However, Fujii *et al.* also report that the tautomeric form of anthrone, 9-anthrol, is emissive. In benzene the spectra are almost identical to the ACRSA emission in MCH: well structured with similar vibronic contributions. Moreover, 9-anthrol in strongly basic solvents (NaOH) emits with a broad Gaussian band, centered at *ca.* 550 nm, very similar to ACRSA in toluene. This shows that charge transfer is

https://dx.doi.org/10.1021/acs.jpclett.0c03314
J. Phys. Chem. Lett. 2021, 12, 1490−1500

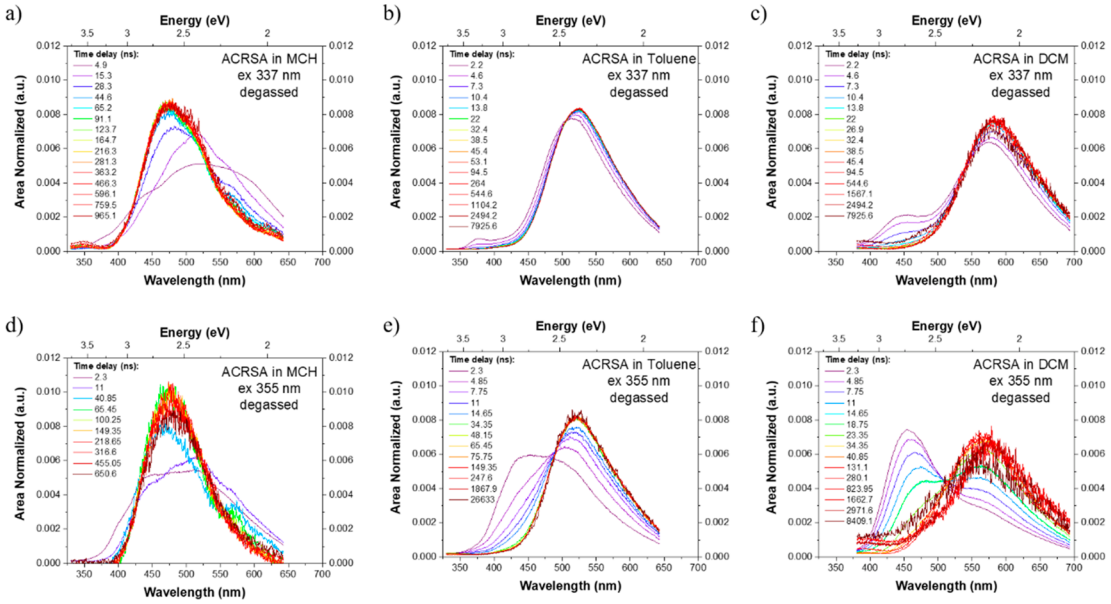

Figure 5. Area-normalized time-resolved emission decay of ACRSA in degassed MCH (a), toluene (b), and DCM (c) solutions (50 μM) excited at 337 nm into the 1^1B_1 exciton transition and at 355 nm into the direct mixed 2^1A_2 and 1^1A_2 transitions (d–f). Poor solubility in MCH leads to the observed emission from dimer/excimer states at long wavelengths. A corresponding set of peak normalized spectra are given in Supporting Figure S13.

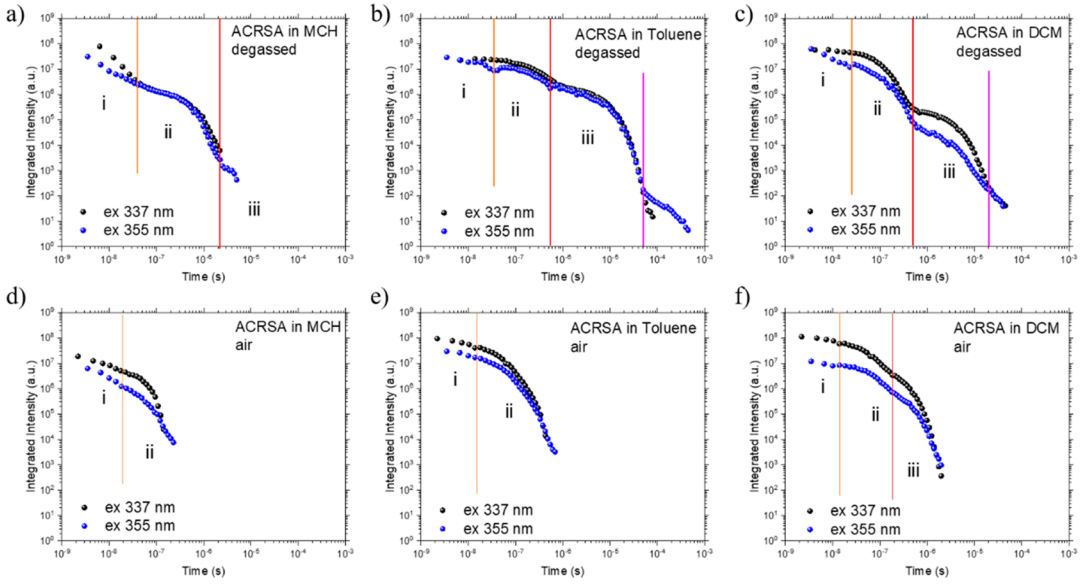

Figure 6. Emission decay kinetics for ACRSA in MCH (a), toluene (b), and DCM (c) (50 μM) as a function of excitation wavelength. Three main kinetic decay regions can be defined for (i) fast ^1LE_A state decay, (ii) slow prompt ^1CT decay, and (iii) delayed ^1CT decay. Panels d, e, and f show the effect of oxygen quenching on the kinetic decays (in aerated solvents).

efficient in ACRSA and that even in the excited state, the D and A units are strongly decoupled. It may also highlight the mixed nature of the excited states (local and CT) and also possible similarities between the excited-state structure of the A unit in ACRSA and that of 9-anthrol. However, this cannot come from such a tautomeric form as proton transfer is impossible for the anthracenone unit that is spiro linked to the acridine in ACRSA.

We observe the largest ^1CT DF emission contribution in toluene (Supporting Figures S10 and 11). The oxygen-dependent spectra in MCH and DCM (Supporting Figure S12) show that exciting into the ^1LE_D exciton leads to an oxygen-dependent CT population (DF increasing by a factor 4 in MCH and 2 in DCM), whereas *via* direct excitation the increase in CT emission is only a factor of 2 in MCH and DCM. This clearly indicates that ^1CT is populated significantly through the triplet manifold and most efficiently *via* the ^1LE_D state.

Time-resolved emission was measured following excitation at both 337 and 355 nm (Figure 5), starting with (degassed) toluene solution. The 337 nm pulses excite the ^1LE_D excitonic state and produce rapidly decaying emission from this state at 370 nm, within the time response of the laser/iCCD system (<1 ns). ^1CT emission is also observed in the earliest spectrum (2 ns), indicating an ET rate (estimated at 10^8–10^9 s^{-1}) that does not out-compete radiative decay and IC of the ^1LE_D state

https://dx.doi.org/10.1021/acs.jpclett.0c03314
J. Phys. Chem. Lett. 2021, 12, 1490–1500

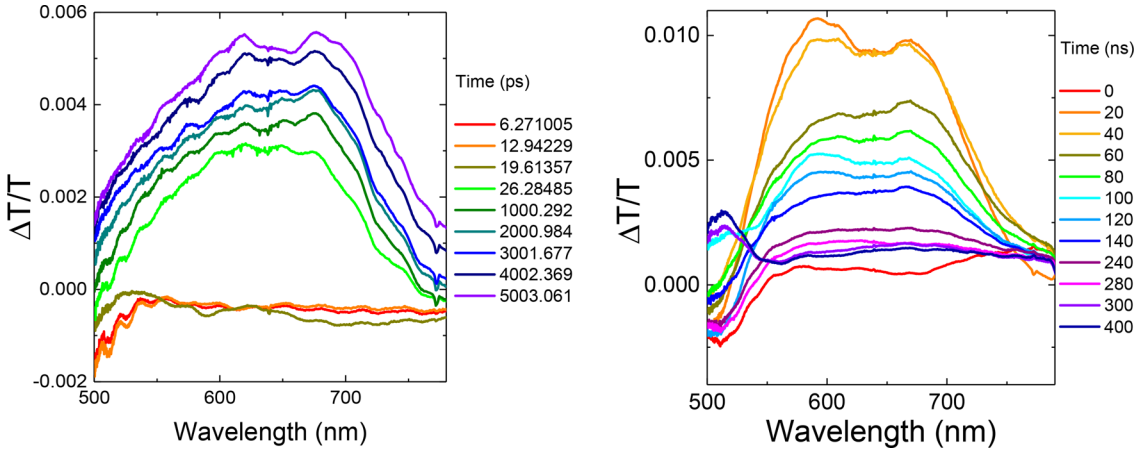

Figure 7. Nanosecond transient absorption spectra of ACRSA in toluene (1 mg/mL) from 0 to 5 ns following 343 nm excitation (left panel) and 0−400 ns following 355 nm excitation (right panel).

but is faster than our time resolution. This relatively slow ET is consistent with the strongly decoupled D and A electronic systems through their near perfect orthogonality. A blue-edge shoulder on the CT emission band indicates a small contribution from ^1LE_A nπ^* emission as well, confirming that the ^1LE_D exciton couples to both lower-lying singlet states.

In all solvents we observe little energy relaxation of the ^{1}CT state with time, indicating a rigid dihedral angle with little dispersion of the ^{1}CT state energy. From the kinetic decay traces in toluene (Figure 6), we observe that the lifetime of the ^1LE_A nπ^* state is very short, of order 2 ns (beginning of region i). Because this emission is a nominally forbidden transition, the short lifetime implies a rapid parallel quenching mechanism, most likely ISC. The prompt CT emission (region ii) is much longer, 274 ± 5 ns.[32] Comparing decays using 337 and 355 nm excitation, we observe stronger coupling of the high-energy excitonic state to the ^{1}CT state giving relatively more ^{1}CT prompt emission. Moreover, delayed CT emission from following 337 nm excitation starts to contribute at rather early times, from *ca.* 600 ns until beyond 10 μs (region iii) with a lifetime of 5.21 ± 0.02 μs, implying a rapid buildup of triplet population. In contrast, excitation at 355 nm directly into the ^1LE_A/ ^{1}CT bands gives more intense local ^1LE_A emission at early times with lifetime *ca.* 5 ns (more pronounced region i). Long-lived prompt ^{1}CT emission, 264 ± 5 ns, and DF lifetime of 5.23 ± 0.06 μs are observed. Kinetic modeling[32] gives rISC rates of 5.29 × 10^5 and 6.2 × 10^5 s^{-1}, respectively, with all kinetic data summarized in Supporting Table 1. Isoemissive points in the time-resolved area-normalized emission spectra (Figure 5) indicate that the ^1LE_A and ^{1}CT states decay independently of each other, consistent with simultaneous photoexcitation but no IC, electron or energy transfer, or vibronic coupling between them. This all indicates very slow radiative decay rates from the CT state consistent with a forbidden transition. This slow decay also demonstrates that ISC to the isoenergetic ^{3}CT is highly forbidden, as there are no close-lying local triplet states to mediate ISC to the ^{3}CT. Nonradiative decay must also be strongly suppressed, indicating few coupling vibrational modes to mediate IC.

In DCM excitation at both 337 and 355 nm photoexcites a much larger initial ^1LE_A population than in toluene, which is not well-structured (in line with the steady-state measurements). The ^1LE_A emission also persists for longer, 10 and 16 ns, respectively. This increase in lifetime reflects a potential blue shift of the ^1LE_A nπ^* and red shift of ^3LE_A $\pi\pi^*$ with increasing solvent polarity, reducing the ISC rate between them. The total emission intensity is however much lower in DCM than in either toluene or MCH, which may result from increased nonradiative quenching of the lower-energy ^{1}CT and ^{3}CT states (energy gap law). In comparson with the decay kinetics in toluene (Figure 6), at 355 nm excitation the prompt ^{1}CT state decays much more rapidly than in toluene (91 ± 3 ns). The DF component in DCM dominates emission after 300 ns (lifetime 2.38 ± 0.06 μs) and has a slower ISC rate (1.18 × 10^6 s^{-1}) than in toluene. The rISC rate is also slower at 4.83 × 10^5 s^{-1}. The CT triplet state involved in rISC, which relaxes in energy with increasing polarity, must therefore open up the gap between itself and the TADF-mediating local triplet state, reducing the rate of rISC and thus DF contribution in polar DCM.[26] In toluene the DF is much stronger but the rISC rate is similar, again indicative of the lower-energy DCM CT states experiencing increased nonradiative decay (energy gap law). The faster radiative decay rates calculated in DCM compared to toluene coupled with the lower overall emission intensity is also explained by an increased nonradiative decay rate; our kinetic model assumes no nonradiative decay (other than ISC) and the fitted "radiative" rate will include both radiative and nonradiative rates.

In MCH the picture is different again. As the ^{1}CT and ^1LE_A nπ^* states are much closer in energy, it is difficult to deconvolute the behavior of each. From the decay kinetics, the ^1LE_A nπ^* decays very rapidly as in toluene, with lifetime of *ca.* 1−2 ns. The prompt CT states decay much faster; the prompt CT lifetime between 5 and 8 ns indicates rapid radiative decay (rates of 4 to 8 × 10^7 s^{-1}) of the ^{1}CT state because of its high LE character (structured emission, Figure 4a[33]). The DF also decays rapidly over only a few microseconds, with a lifetime of *ca.* 350 ns. With 337 nm excitation (Figure 6 and Supporting Figure S13), in the first 10 ns emission covers the whole spectral window between 360 and 650 nm. This we assume is simultaneous emission from multiple excited states, along with possible aggregate emission. Even at early times, the ^{1}CT emission is much stronger than that from the local ^1LE_A nπ^* state. All of these states decay rapidly leaving just the main ^{1}CT emission, as seen in the steady-state emission.

Phosphorescence was collected from ACRSA in a zeonex polymer matrix at 80 K (Supporting Figure S14). From this we deduce that the lowest-energy triplet state is of local character,

https://dx.doi.org/10.1021/acs.jpclett.0c03314
J. Phys. Chem. Lett. 2021, 12, 1490−1500

with energy 2.88 eV (0−0 vibronic peak) and well-resolved structure. From the spectral shape we conclude that the emission emanates from the acceptor anthracenone unit, *i.e.*, ^3LE_A nπ^* state. At very long delay times (80 ms) we observe the emergence of another phosphorescence band. With little structure and onset of 3.2 eV, this matches well with reported acridine phosphorescence.[25] Such dual phosphorescence was previously reported by us in other TADF D−A systems arising from a thermal equilibrium between D and A triplet states which are vibrationally coupled.[26,34] The observation of dual phosphorescence establishes ACRSA as an anti-Kasha material on the triplet manifold in addition to its profoundly anti-Kasha singlet behavior.

We also examine the effect of oxygen quenching on the emission dynamics (Figure 6 and Supporting Figure S18). In toluene and DCM the early time emission spectra and decays are unaffected by oxygen, as would be expected from prompt emitting states, but lifetimes are a little longer, which we have no clear idea about at this time. In toluene, the prompt CT emission is quenched after *ca.* 36 μs (presumably by oxygen), but we observe weak DF, lifetime of *ca.* 120−240 ns accounting for about 5% of the total intensity. It is therefore remarkable to observe DF CT emission for such a long time in air.

Figure 7 shows transient absorption spectra of ACRSA in oxygen-free toluene for the first 6 ns (343 nm excitation) and 400 ns after pump (355 nm excitation). A band centered at 620 nm is seen to grow in after an induction time of ∼25 ps. The induced band can be resolved into two peaks centered at 619 and at 675 nm. Both of these peaks have the same decay kinetics, with the entire band growing in for ∼8−10 ns and decaying after ∼200 ns. Estimation of the band edge energy of each peak (assuming a Gaussian peak shape) yields energies of 1.84 and 1.65 eV, giving an energy separation of 190 meV, corresponding precisely with the C=O stretch of anthracenone. This is also the mode that vibronically couples the LE and CT triplet states.[35]

As the induced absorption has a lifetime of 200 ns it cannot correspond to transitions from the short-lived local singlet ^1LE_D or ^1LE_A states. It also cannot be a transition from the long-lived (>3 μs) $^{1/3}$CT population, and the ^{1}CT emission energy is too low to accommodate an induced absorption at the observed energies. By elimination, this induced absorption is assigned to a transition from a ^{3}LE triplet state. Supporting this, measurements in aerated solution gave very poor signal, consistent with oxygen quenching of triplet states. The grow-in kinetics of this induced band matches well with the fast decay of the local ^1LE_D state with 343 nm excitation. We thus conclude that the induced absorption comes from a transient ^3LE_A $\pi\pi^*$ population, having lifetime of ∼200 ns as it undergoes subsequent IC to the lower energy ^3LE_A $n\pi^*$ triplet state. With excitation at 355 nm we initially populate the ^1LE_A nπ^* state which rapidly undergoes ISC to populate the ^3LE_A $\pi\pi^*$. In both cases we observe the same photoinduced absorption spectra, confirming the common ^3LE_A $\pi\pi^*$ assignment. The induction time observed with 343 nm excitation corresponds to the slower ISC and subsequent IC steps required to reach the ^3LE_A $\pi\pi^*$ state from the ^1LE_D (ISC to ^3LE_D then IC). At low temperatures when vibrational coupling and ISC/IC are inefficient, these $^1LE_{D/A}$ states give rise to the observed dual phosphorescence.

The molecular photophysics of TADF in ACRSA is substantially different from that of established TADF molecules, with different ISC and rISC channels.[36] Strong solvatochromic relaxation of the lowest-energy singlet ^{1}CT state occurs, while a close-lying ^1LE_A nπ^* state remains unaffected by polarity. Both of these A_2 states are emissive despite being one-photon symmetry forbidden. The ^1LE_A nπ^* is quenched to its ^{3}LE $\pi\pi^*$ triplet state through very fast ISC in accordance with El Sayed's rule. In transient absorption a rapid grow-in of a ^{3}LE $\pi\pi^*$ induced absorption is in agreement with this explanation. This ISC step out competes any vibrational coupling to the ^{1}CT state, as confirmed by the time-resolved emission spectra showing that these states decay independently. In MCH the ^{1}CT state has strong LE character giving fast radiative decay rates and a short PF CT lifetime compared to toluene and DCM (Supporting Table 1). The PF CT emission has a long lifetime in toluene and DCM because the ^{1}CT state is energetically distant from the ^1LE_A nπ^* state, precluding second-order vibronic coupling to any local state (singlet or triplet). This, along with the forbidden nature of direct ^{1}CT to ^{3}CT SOC, is clearly observed through the extremely long ^{1}CT lifetime. In DCM, the CT states shift so low in energy that coupling to the ground state increases nonradiative decay (energy gap law). However, the presence of TADF in all solvents confirms that isolation of the ^{1}CT is not important in the formation of a long-lived ^{3}CT population because of the role of the ^1LE_A nπ^* state.

Optically the DF emission intensity is low in MCH despite more appropriate energy level ordering. This we suggest is due to rISC from the ^{3}CT state being in continuous competition with IC back to the strongly coupled ^3LE_A nπ^* state. This is also why we can observe resolved phosphorescence from this local triplet state. In MCH we do still identify a fast DF signal quenched by oxygen. This confirms the strong enhancement of both radiative decay and rISC in MCH, achieved through near resonant ^{1}CT and ^{3}CT states (with high local character) and closely spaced ^1LE_A $\pi\pi^*$ singlet, ^3LE_A $\pi\pi^*$, and ^3LE_A nπ^* triplet states. This alignment of energy levels yields both small energy gaps for efficient nonadiabatic vibronic coupling and large SOC matrix elements, giving very fast rISC rate of $\sim 1 \times 10^7$ s^{-1}. This fast rISC rate is required for it to compete with rapid IC to the well-coupled lowest-energy ^3LE_A nπ^* state.

As the polarity of the solvent increases ^{1}CT and ^{3}CT energetically relax, with ^{3}CT becoming the lowest-energy triplet state. A larger gap opens to the local states especially to the ^3LE_A nπ^*, which increases in energy with increasing solvent polarity, as observed in other aromatic ketone systems.[37,38] The measured rISC rates consequently fall by nearly 2 orders of magnitude with increasing polarity (Supporting Table 1), reflecting the increasing energy gap between ^{3}CT and local states (but uniform energy gaps between the local singlet and triplet acceptor states).[39] The highly structured phosphorescence from the anthracenone acceptor unit indicates that in nonpolar solvents the ^3LE_A nπ^* triplet state must be below the TADF-active ^{3}CT state.

In all solvents we never observe DF from the ^1LE_A nπ^*, but we do observe dual ^1LE_A nπ^* and ^{1}CT emission. This clearly indicates the two states are decoupled. In MCH we see that the ^1LE_A nπ^* and unrelaxed ^{1}CT energies are very close, resulting in a very low driving force for ET from the ^1LE_A nπ^* state insufficient to drive charge transfer, especially in competition with fast quenching by ISC.

https://dx.doi.org/10.1021/acs.jpclett.0c03314
J. Phys. Chem. Lett. 2021, 12, 1490−1500

From the time-resolved emission spectra (Figure 5) it is clear that in all solvents the CT state that gives prompt and DF emission does not red shift significantly with time. This emission is also relatively narrow, indicating solvent shell reorganization is very fast and there is no electronic relaxation of the CT state caused by slow molecular reorganization.[40,41]

ACRSA is unique in that it allows excitation into more than one singlet state. Below 350 nm, excitation of the ^1LE_D $\pi\pi^*$ exciton yields fast emission from this high-energy excitonic singlet state observed in aerated solutions, in competition with electron transfer to create the ^1CT state. However, the main deactivation pathway of the ^1LE_D $\pi\pi^*$ exciton is *via* ISC to upper triplet states, which then decay down the triplet manifold to populate ^3CT triplet states, yielding DF from subsequent rISC. This is confirmed by the strong oxygen dependence of the DF CT emission we observe and the results from photoinduced absorption measurements. Nonradiative decay can occur *via* other triplet states that do not couple to the rISC-active lowest-energy CT triplet state, leading to excited-state quenching. Excitation above 350 nm directly populates the ^1CT and ^1LE_A nπ^* excitonic states, yielding simultaneous prompt emission from both states.

These results confirm the very fast ISC channel from ^1LE_A nπ^* to ^3LE_A $\pi\pi^*$ in ACRSA, as predicted by Lyskov and Marian. rISC remains much slower than this in polar solvents, typically with 2−5 μs lifetime. However, in MCH far higher rISC rates are seen as the TADF-active ^3CT state rises in energy toward the ^3LE states.[24]

This leads us to a proposed "experimental" energy level scheme given in Figure 8, based on the calculations of Lyskov and Marian and our experimental observations.

Combining all of our experimental observations we conclude the following ISC and rISC channels populate the CT states in ACRSA *via* direct optical excitation of the ^1LE_A nπ^*.

^1LE_A nπ^* ISC channel:

$$^1LE_A\ n\pi^* \xrightarrow{SOC} {}^3LE_A\ \pi\pi^* \xrightarrow{SOC} {}^3LE_A\ n\pi^* \xrightarrow{Vib} {}^3CT\ \pi\pi^*$$

^1CT $\pi\pi^*$ rISC channel;

$$^3CT\ \pi\pi^* \xrightarrow{Vib} {}^3LE_A\ n\pi^* \xrightarrow{SOC} {}^1CT\ \pi\pi^*$$

We observe that the ^1LE_A nπ^* and $\pi\pi^*$ singlet states are not affected by polarity, but from calculation and reports of other ketones, the triplet nπ^* states are more affected, shifting up in energy, which we depict in Figure 7. Thus, the SOC step *via* ^3LE_A $\pi\pi^*$ states should be minimally affected by polarity changes. The rate-limiting step is likely the ^3CT coupling to the ^3LE_A nπ^* through vibronic coupling and so is not as impacted by the increasing energy gap in toluene and DCM. The overall rISC rate is controlled by this vibronic coupling, decreasing rISC rates in toluene and DCM compared to MCH from 10^7 s^{-1} to *ca.* 5×10^5 s^{-1}. In air we observe ^1CT quenching because of the very long natural lifetime in toluene and DCM. We propose this simpler rISC mechanism compared to that of Lyskov and Marian because we never observe delayed emission from the ^1LE_A nπ^* state.

In this study, the "simple" spiro TADF molecule ACRSA is demonstrated to be anything but. We find both strong excitation energy and solvent polarity dependencies in its emission. Exciting the first allowed local $\pi\pi^*$ excitonic state of the donor acridine gives rise to three different emissions: one from the excitonic state itself (that competes with both ISC and IC, and electron transfer to two lower lying, one-photon forbidden A_2 symmetry states), one from the local nπ^* state of the anthracenone acceptor, and also emission from a CT state. Dual emission from these symmetry forbidden (A_2) states is indicative of mixing with the donor excitonic states in ACRSA. These lower energy states have weak direct absorption giving rise to prompt local ^1LE_A nπ^* state emission and both prompt and delay CT emission. On the removal of oxygen, we observe very large increases in the emission from the CT state, indicating a large delayed emission contribution. We find no

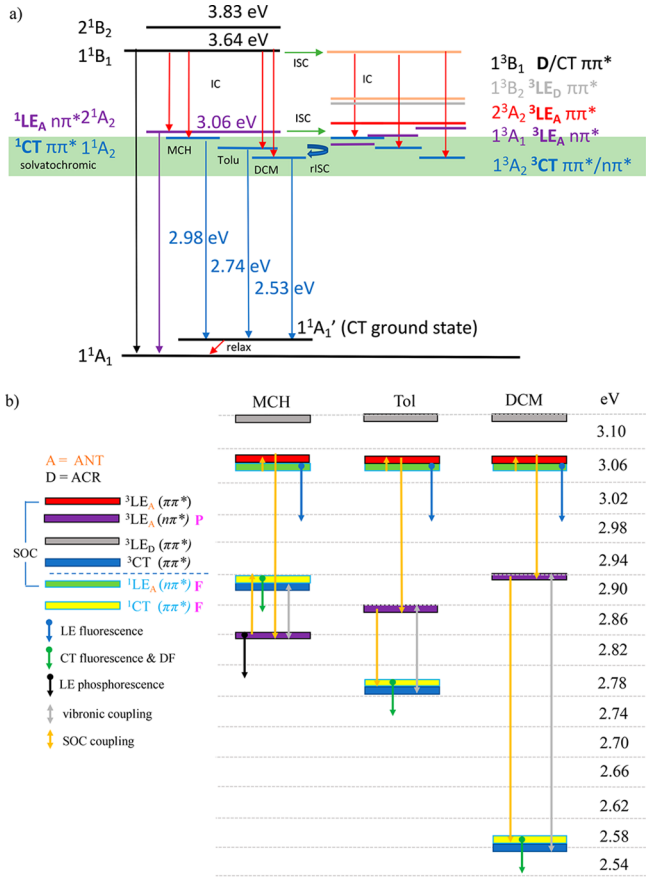

20

Figure 8. Energy level scheme for ACRSA. (a) Measured energy levels from spectral onsets of ACRSA in different polarity solvents, following the nomenclature of Lyskov and Marian.[24] The green band represents the energy range over which we observe solvatochromic states. Red arrows represent nonradiative transitions. (b) The effect of solvent polarity on the states and the SOC (yellow arrows) and vibronic coupling (gray arrows) between states giving rise to ISC and rISC.

In this study, the "simple" spiro TADF molecule ACRSA is demonstrated to be anything but. We find both strong excitation energy and solvent polarity dependencies in its emission.

https://dx.doi.org/10.1021/acs.jpclett.0c03314
J. Phys. Chem. Lett. 2021, 12, 1490−1500

DF from the ^1LE_A nπ^* state however. Both direct and indirect excitation (*via* the excitonic state) gives very large DF emission in degassed solutions.

In agreement with DFT/MRCI calculations, fast ISC between the lowest-energy ^1LE_A nπ^* singlet state and ^3LE_A $\pi\pi^*$ triplet state is established from the correspondence of ^1LE_A nπ^* emission decay and grow-in of induced absorption from the ^3LE_A $\pi\pi^*$ state, confirming strong SOC between these states. In MCH we observe very strong enhancement of both radiative decay and rISC, achieved through near-resonant ^{1}CT and ^{3}CT states (having high local character) as well as nearby ^{1}LE nπ^* singlet and ^{3}LE $\pi\pi^*$ triplet states. This alignment yields high radiative decay rates for the ^{1}CT state, small energy gaps for nonadiabatic vibronic coupling, and high SOC rates. The net result is very high rISC rates of 10^7 s^{-1}. However, rapid ISC from excitation to higher-energy singlet states yields fewer triplet states and lower DF. This indicates competing decay channels on the triplet manifold, with not all excitons reaching the lowest-energy TADF-active triplet state. In devices, similar ISC from high-energy excitons terminating in TADF-inactive triplet states may be a mechanism that explains the generally unexceptional OLED performance of ACRSA and other spiro-linked derivatives.

Throughout our optical measurements ACRSA gives radiative decay from up to three different excited states simultaneously (at early times) and two states even at tens of nanoseconds. Combined with observed dual phosphorescence this "simple" molecule therefore utterly disregards Kasha's law. The perpendicular and rigid geometry of the molecule—which very effectively decouples A and D as required—is what allows us to see identifiable photophysical properties of the donor (^1LE_D $\pi\pi^*$ exciton emission, in competition with slow ET and nonradiative decay), alongside formally forbidden ^{1}CT and ^1LE_A nπ^* emission. ACRSA's "simple" spiro structure therefore bestows it with unprecedented and previously unrecognized richness in its optical properties because of this very effective electronic decoupling of the donor and acceptor units, apart from the molecular CT state. This is not limited to ACRSA, nor spiro TADF molecules in general, but all TADF molecules because of the requirement to effectively decouple the D and A to yield CT states with vanishing singlet−triplet energy gaps, a necessary (but not sufficient) requirement for efficient TADF. This whole class of materials can be thought of as a combination of donor, acceptor, and molecular CT state giving their own photophysics, as is the case for an exciplex TADF systems[10,42] and emerging through-space TADF materials, where the linkage and coupling between the D and A is even less well-defined. Thus, in its original form, does Kasha's rule still apply to such a "system"?

■ ASSOCIATED CONTENT

Supporting Information

The Supporting Information is available free of charge at https://pubs.acs.org/doi/10.1021/acs.jpclett.0c03314.

Experimental details; additional photophysical data such as absorption spectra, time-resolved emission decays and steady-state spectra of ACRSA in different solvents, excitation, and concentrations; phosphorescence spectra of ACRSA in zeonex matrix; absorption and emission spectra of acridine; lifetime fittings (PDF)

■ AUTHOR INFORMATION

Corresponding Author

Andrew Monkman − *OEM Research Group, Department of Physics, Durham University, Durham DH1 3LE, United Kingdom;* orcid.org/0000-0002-0784-8640; Email: a.p.monkman@durham.ac.uk

Authors

Larissa Gomes Franca − *OEM Research Group, Department of Physics, Durham University, Durham DH1 3LE, United Kingdom*

Yun Long − *OEM Research Group, Department of Physics, Durham University, Durham DH1 3LE, United Kingdom*

Chunyong Li − *OEM Research Group, Department of Physics, Durham University, Durham DH1 3LE, United Kingdom*

Andrew Danos − *OEM Research Group, Department of Physics, Durham University, Durham DH1 3LE, United Kingdom;* orcid.org/0000-0002-1752-8675

Complete contact information is available at: https://pubs.acs.org/10.1021/acs.jpclett.0c03314

Author Contributions

L.G.F., Y.L., A.D., and C.L. made the presented optical and time-resolved spectroscopy measurements. A.M. devised the research, undertook the data analysis, and supervised the work. A.M. wrote the manuscript with L.G.F. and A.D., with contributions from all authors.

Notes

The authors declare no competing financial interest.

■ ACKNOWLEDGMENTS

We thank the EPSRC (EP/P012167/1) and acknowledge the TADFlife and HyperOLED projects funded by the European Union's Horizon 2020-MCSA-ITN Research and Innovation Programme under Grant Agreements No. 812872 and No. 732013 under the action ICT-02-2016 for funding the research in Durham. We acknowledge fruitful conversations with Professor C. Marian.

■ REFERENCES

(1) Mizukami, M.; Cho, S. Il; Watanabe, K.; Abiko, M.; Suzuri, Y.; Tokito, S.; Kido, J. Flexible Organic Light-Emitting Diode Displays Driven by Inkjet-Printed High-Mobility Organic Thin-Film Transistors. *IEEE Electron Device Lett.* **2018**, *39*, 39−42.

(2) Huang, T.; Jiang, W.; Duan, L. Recent Progress in Solution Processable TADF Materials for Organic Light-Emitting Diodes. *J. Mater. Chem. C* **2018**, *6*, 5577−5596.

(3) Forrest, S. R. The Path to Ubiquitous and Low-Cost Organic Electronic Appliances on Plastic. *Nature* **2004**, *428*, 911−918.

(4) Kim, J. J.; Han, M. K.; Noh, Y. Y. Flexible OLEDs and Organic Electronics. *Semicond. Sci. Technol.* **2011**, *26*, 030301.

(5) Baldo, M. A.; O'Brien, D. F.; You, Y.; Shoustikov, A.; Sibley, S.; Thompson, M. E.; Forrest, S. R. Highly Efficient Phosphorescent Emission from Organic Electroluminescent Devices. *Nature* **1998**, *395*, 151−154.

(6) Adachi, C.; Baldo, M. A.; Thompson, M. E.; Forrest, S. R. Nearly 100% Internal Phosphorescence Efficiency in an Organic Light-Emitting Device. *J. Appl. Phys.* **2001**, *90*, 5048−5051.

(7) Shizu, K.; Uejima, M.; Nomura, H.; Sato, T.; Tanaka, K.; Kaji, H.; Adachi, C. Enhanced Electroluminescence from a Thermally Activated Delayed-Fluorescence Emitter by Suppressing Nonradiative Decay. *Phys. Rev. Appl.* **2015**, *3*, 014001.

(8) Uoyama, H.; Goushi, K.; Shizu, K.; Nomura, H.; Adachi, C. Highly Efficient Organic Light-Emitting Diodes from Delayed Fluorescence. *Nature* **2012**, *492*, 234−238.
(9) Dias, F. B.; Bourdakos, K. N.; Jankus, V.; Moss, K. C.; Kamtekar, K. T.; Bhalla, V.; Santos, J.; Bryce, M. R.; Monkman, A. P. Triplet Harvesting with 100% Efficiency by Way of Thermally Activated Delayed Fluorescence in Charge Transfer OLED Emitters. *Adv. Mater.* **2013**, *25*, 3707−3714.
(10) Colella, M.; Danos, A.; Monkman, A. P. Less Is More: Dilution Enhances Optical and Electrical Performance of a TADF Exciplex. *J. Phys. Chem. Lett.* **2019**, *10*, 793−798.
(11) Im, Y.; Kim, M.; Cho, Y. J.; Seo, J.-A.; Yook, K. S.; Lee, J. Y. Molecular Design Strategy of Organic Thermally Activated Delayed Fluorescence Emitters. *Chem. Mater.* **2017**, *29*, 1946−1963.
(12) Stachelek, P.; Ward, J. S.; Dos Santos, P. L.; Danos, A.; Colella, M.; Haase, N.; Raynes, S. J.; Batsanov, A. S.; Bryce, M. R.; Monkman, A. P. Molecular Design Strategies for Color Tuning of Blue TADF Emitters. *ACS Appl. Mater. Interfaces* **2019**, *11*, 27125.
(13) Huang, R.; Kukhta, N. A.; Ward, J. S.; Danos, A.; Batsanov, A. S.; Bryce, M. R.; Dias, F. B. Balancing Charge-Transfer Strength and Triplet States for Deep-Blue Thermally Activated Delayed Fluorescence with an Unconventional Electron Rich Dibenzothiophene Acceptor. *J. Mater. Chem. C* **2019**, *7*, 13224−13234.
(14) Lim, B. T.; Okajima, S.; Chandra, A. K.; Lim, E. C. Radiationless Transitions in Electron Donor-Acceptor Complexes: Selection Rules for S1 → T Intersystem Crossing and Efficiency of S1 → S0 Internal Conversion. *Chem. Phys. Lett.* **1981**, *79*, 22−27.
(15) Gibson, J.; Monkman, A. P.; Penfold, T. J. The Importance of Vibronic Coupling for Efficient Reverse Intersystem Crossing in Thermally Activated Delayed Fluorescence Molecules. *ChemPhysChem* **2016**, *17*, 2956−2961.
(16) Hatakeyama, T.; Shiren, K.; Nakajima, K.; Nomura, S.; Nakatsuka, S.; Kinoshita, K.; Ni, J.; Ono, Y.; Ikuta, T. Ultrapure Blue Thermally Activated Delayed Fluorescence Molecules: Efficient HOMO-LUMO Separation by the Multiple Resonance Effect. *Adv. Mater.* **2016**, *28*, 2777−2781.
(17) Romanov, A. S.; Jones, S. T. E.; Gu, Q.; Conaghan, P. J.; Drummond, B. H.; Feng, J.; Chotard, F.; Buizza, L.; Foley, M.; Linnolahti, M.; Credgington, D.; Bochmann, M. Carbene Metal Amide Photoemitters: Tailoring Conformationally Flexible Amides for Full Color Range Emissions Including White-Emitting OLED. *Chem. Sci.* **2020**, *11*, 435−446.
(18) Hall, D.; Suresh, S. M.; dos Santos, P. L.; Duda, E.; Bagnich, S.; Pershin, A.; Rajamalli, P.; Cordes, D. B.; Slawin, A. M. Z.; Beljonne, D.; Köhler, A.; Samuel, I. D. W.; Olivier, Y.; Zysman-Colman, E. Improving Processability and Efficiency of Resonant TADF Emitters: A Design Strategy. *Adv. Opt. Mater.* **2020**, *8*, 1901627.
(19) Méhes, G.; Nomura, H.; Zhang, Q.; Nakagawa, T.; Adachi, C. Enhanced Electroluminescence Efficiency in a Spiro-Acridine Derivative through Thermally Activated Delayed Fluorescence. *Angew. Chem., Int. Ed.* **2012**, *51*, 11311−11315.
(20) Nakagawa, T.; Ku, S. Y.; Wong, K. T.; Adachi, C. Electroluminescence Based on Thermally Activated Delayed Fluorescence Generated by a Spirobifluorene Donor−Acceptor Structure. *Chem. Commun.* **2012**, *48*, 9580−9582.
(21) Ohkuma, H.; Nakagawa, T.; Shizu, K.; Yasuda, T.; Adachi, C. Thermally Activated Delayed Fluorescence from a Spiro-Diazafluorene Derivative. *Chem. Lett.* **2014**, *43*, 1017−1019.
(22) Wang, Y. K.; Huang, C. C.; Ye, H.; Zhong, C.; Khan, A.; Yang, S. Y.; Fung, M. K.; Jiang, Z. Q.; Adachi, C.; Liao, L. S. Through Space Charge Transfer for Efficient Sky-Blue Thermally Activated Delayed Fluorescence (TADF) Emitter with Unconjugated Connection. *Adv. Opt. Mater.* **2020**, *8*, 1901150.
(23) Nasu, K.; Nakagawa, T.; Nomura, H.; Lin, C.-J.; Cheng, C.-H.; Tseng, M.-R.; Yasuda, T.; Adachi, C. A Highly Luminescent Spiro-Anthracenone-Based Organic Light-Emitting Diode Exhibiting Thermally Activated Delayed Fluorescence. *Chem. Commun.* **2013**, *49*, 10385.
(24) Lyskov, I.; Marian, C. M. Climbing up the Ladder: Intermediate Triplet States Promote the Reverse Intersystem Crossing in the Efficient TADF Emitter ACRSA. *J. Phys. Chem. C* **2017**, *121*, 21145−21153.
(25) dos Santos, P. L.; Ward, J. S.; Bryce, M. R.; Monkman, A. P. Using Guest−Host Interactions to Optimize the Efficiency of TADF OLEDs. *J. Phys. Chem. Lett.* **2016**, *7*, 3341−3346.
(26) Dias, F. B.; Santos, J.; Graves, D. R.; Data, P.; Nobuyasu, R. S.; Fox, M. A.; Batsanov, A. S.; Palmeira, T.; Berberan-Santos, M. N.; Bryce, M. R.; et al. The Role of Local Triplet Excited States and D-A Relative Orientation in Thermally Activated Delayed Fluorescence: Photophysics and Devices. *Adv. Sci.* **2016**, *3*, 1600080.
(27) Huang, R.; Ward, J. S.; Kukhta, N. A.; Avó, J.; Gibson, J.; Penfold, T.; Lima, J. C.; Batsanov, A. S.; Berberan-Santos, M. N.; Bryce, M. R.; et al. The Influence of Molecular Conformation on the Photophysics of Organic Room Temperature Phosphorescent Luminophores. *J. Mater. Chem. C* **2018**, *6*, 9238−9247.
(28) Ward, J. S.; Nobuyasu, R. S.; Fox, M. A.; Batsanov, A. S.; Santos, J.; Dias, F. B.; Bryce, M. R. Bond Rotations and Heteroatom Effects in Donor−Acceptor−Donor Molecules: Implications for Thermally Activated Delayed Fluorescence and Room Temperature Phosphorescence. *J. Org. Chem.* **2018**, *83*, 14431−14442.
(29) Nobuyasu, R. S.; Ward, J. S.; Gibson, J.; Laidlaw, B. A.; Ren, Z.; Data, P.; Batsanov, A. S.; Penfold, T. J.; Bryce, M. R.; Dias, F. B. The Influence of Molecular Geometry on the Efficiency of Thermally Activated Delayed Fluorescence. *J. Mater. Chem. C* **2019**, *7*, 6672−6684.
(30) Ward, J. S.; Nobuyasu, R. S.; Fox, M. A.; Aguilar, J. A.; Hall, D.; Batsanov, A. S.; Ren, Z.; Dias, F. B.; Bryce, M. R. Impact of Methoxy Substituents on Thermally Activated Delayed Fluorescence and Room-Temperature Phosphorescence in All-Organic Donor-Acceptor Systems. *J. Org. Chem.* **2019**, *84*, 3801−3816.
(31) Fujii, T.; Mishima, S.; Tanaka, N.; Kawauchi, O.; Kodaira, K.; Nishikiori, H.; Kawai, Y. Absorption and Fluorescence Spectra of 9-Anthrol and Its Chemical Species in Solution. *Res. Chem. Intermed.* **1997**, *23*, 829−839.
(32) Haase, N.; Danos, A.; Pflumm, C.; Morherr, A.; Stachelek, P.; Mekic, A.; Brütting, W.; Monkman, A. P. Kinetic Modeling of Transient Photoluminescence from Thermally Activated Delayed Fluorescence. *J. Phys. Chem. C* **2018**, *122*, 29173−29179.
(33) De Sa Pereira, D.; Menelaou, C.; Danos, A.; Marian, C.; Monkman, A. P. Electroabsorption Spectroscopy as a Tool for Probing Charge Transfer and State Mixing in Thermally Activated Delayed Fluorescence Emitters. *J. Phys. Chem. Lett.* **2019**, *10*, 3205−3211.
(34) Nobuyasu, R. S.; Ren, Z.; Griffiths, G. C.; Batsanov, A. S.; Data, P.; Yan, S.; Monkman, A. P.; Bryce, M. R.; Dias, F. B. Rational Design of TADF Polymers Using a Donor-Acceptor Monomer with Enhanced TADF Efficiency Induced by the Energy Alignment of Charge Transfer and Local Triplet Excited States. *Adv. Opt. Mater.* **2016**, *4*, 597−607.
(35) Marian, C. M. Mechanism of the Triplet-to-Singlet Upconversion in the Assistant Dopant ACRXTN. *J. Phys. Chem. C* **2016**, *120*, 3715−3721.
(36) Etherington, M. K.; Gibson, J.; Higginbotham, H. F.; Penfold, T. J.; Monkman, A. P. Revealing the Spin−Vibronic Coupling Mechanism of Thermally Activated Delayed Fluorescence. *Nat. Commun.* **2016**, *7*, 13680.
(37) Mundt, R.; Villnow, T.; Ziegenbein, C. T.; Gilch, P.; Marian, C.; Rai-Constapel, V. Thioxanthone in Apolar Solvents: Ultrafast Internal Conversion Precedes Fast Intersystem Crossing. *Phys. Chem. Chem. Phys.* **2016**, *18*, 6637−6647.
(38) Rai-Constapel, V.; Villnow, T.; Ryseck, G.; Gilch, P.; Marian, C. M. Chimeric Behavior of Excited Thioxanthone in Protic Solvents: II. Theory. *J. Phys. Chem. A* **2014**, *118*, 11708−11717.
(39) Dias, F. B.; Penfold, T. J.; Monkman, A. P. Photophysics of Thermally Activated Delayed Fluorescence Molecules. *Methods Appl. Fluoresc.* **2017**, *5*, 012001.

https://dx.doi.org/10.1021/acs.jpclett.0c03314
J. Phys. Chem. Lett. 2021, 12, 1490−1500

(40) Ward, J. S.; Nobuyasu, R. S.; Batsanov, A. S.; Data, P.; Monkman, A. P.; Dias, F. B.; Bryce, M. R. The Interplay of Thermally Activated Delayed Fluorescence (TADF) and Room Temperature Organic Phosphorescence in Sterically-Constrained Donor−Acceptor Charge-Transfer Molecules. *Chem. Commun.* **2016**, *52*, 2612.
(41) Santos, P. L.; Ward, J. S.; Data, P.; Batsanov, A. S.; Bryce, M. R.; Dias, F. B.; Monkman, A. P. Engineering the Singlet−Triplet Energy Splitting in a TADF Molecule. *J. Mater. Chem. C* **2016**, *4*, 3815−3824.
(42) dos Santos, P. L.; Dias, F. B.; Monkman, A. P. Investigation of the Mechanisms Giving Rise to TADF in Exciplex States. *J. Phys. Chem. C* **2016**, *120*, 18259−18267.

https://dx.doi.org/10.1021/acs.jpclett.0c03314
J. Phys. Chem. Lett. 2021, 12, 1490−1500